INO TECH
Inspiring Technologies and Innovations

Inspiring Technologies and Innovations

June 2024, Volume: 3 Issue: 1

Research Article

Spatiotemporal Modeling and Simulation of DC Microplasma Glow Discharges in the ZnSe-Ar/H_2 System

Erhan ONGUN[a], Hatice Hilal YÜCEL (KURT)[b]

[a,b]Gazi University, Graduate School of Natural and Applied Sciences, Department of Physics, TÜRKİYE.

ORCID[a]: 0009-0007-4966-1044
ORCID[b]: 0000-0002-1277-5204

Corresponding Author e-mail: hkurt@gazi.edu.tr

https://doi.org/10.5281/zenodo.12544420

Received	: 25.12.2023	Accepted	: 19.04.2024	Pages	: 01-08

ABSTRACT: With their unique electrical and optical properties, microplasmas have become the focus of great interest in the broad field of plasma science and engineering in designing advanced materials and devices, including light sources, photodetectors, and microplasma field effect transistors. This conceptual research study was carried out for the numerical analyzes of gas discharge-semiconductor microplasma (GDSμP) systems in the COMSOL Multiphysics program. Plasma modeling was based on the electron energy distribution using Maxwell analytic function. Zinc selenide (ZnSe), a type II-VI compound semiconductor, was modeled as the cathode electrode with a micro-digitated electron emission surface, coupled to a micro discharge gap of unary argon (Ar) and binary argon/hydrogen (Ar/H_2) gases. Bandgap tunable ZnSe has attracted the attention of researchers for various optoelectronic applications, including high-efficiency and fast-response infrared imaging devices in the near-to-mid infrared spectrum. The binary gas system consisted of argon mixed with 10% molar hydrogen. Spatiotemporal distribution patterns of the main discharge parameters were plotted across 100 μm long discharge gap of a two-dimensional square chamber in gases media at 250 Torr sub atmospheric pressure. Microscale normal glow discharges were generated under electric field fed with a constant voltage of 1300 VDC in a virtual electrical equivalent circuit (EEC). GDSμP cells were simulated to explore the fast transient discharge parameters, including electron density (ED), electron current density (ECD), and electric potential (EP). It was figured out that microplasma devices combined with gas discharge-semiconductor systems can be specifically designed for infrared detector and image converter applications.

KEYWORDS: Microplasma, zinc selenide, glow discharge, simulation, infrared, image converter.

1. INTRODUCTION

The area of microplasma has become a focus of increasing interest in the plasma science and technology. Microplasmas are non-thermal, high-energy-density and non-equilibrium reactive gas discharge media that feature at least one physical dimension in the micrometer range. Their unique electrical and optical characteristics make microplasmas attractive for designing novel materials and functional devices in various applications, including light sources, photodetectors, and microplasma field effect transistors. Microplasmas are generated by electrical breakdown in gases at sub atmospheric or atmospheric pressures.

A topical review published in the field of microplasma science and technology provided a comprehensive status report into the microplasma research with examples of applications [1]. Recent research works were also reported in the field of microplasma device technology [2,3]. Several theoretical and experimental investigations were reported in the gas discharge-semiconductor microplasma systems (GDSμP) [4]. Direct-current (DC) argon (Ar) glow discharges were experimentally investigated for infrared-to-visible wavelength conversion applications. Nonlinear electrical transport properties were reported for Ar -glow discharges over a wide range of sub atmospheric pressures under various infrared (IR) light illumination intensities on gallium arsenide (GaAs) semiconductor cathode electrode [5,16]. Electron emission mechanisms on microscale gas breakdown were extensively reported [6,7]. The Townsend avalanche governs the ionization process for gases, in which thermofield emission, ion-induced secondary electron emission, and field emission mechanisms are involved. The phenomenon of gas breakdown has also been studied using computational methods [8].

Zinc selenide (ZnSe), a type II-VI compound semiconductor, is a unique bandgap tunable semiconductor material with excellent electronic transport properties and optical transparency in the visible spectrum. ZnSe -based optoelectronic device applications were reviewed in [9,10]. The infrared sensitivity of ZnSe was specifically investigated for the infrared-to-visible conversion device applications [11]. DC -driven Ar -glow discharges in microgaps combined with ZnSe cathode were experimentally explored under atmospheric pressures [12]. The electrical discharge parameters in the ZnSe-Ar/H_2 system were investigated numerically and experimentally at sub atmospheric pressures under infrared illumination [13].

The effect of cathode surface morphology, including intrinsic surface roughness and artificial surface patterning, such as the growth of multiple concentric protrusions, on electron emission mechanisms was examined [14,15].

Figure 1 shows the schematic representation of GDSS cell for the infrared-to-visible wavelength conversion device application.

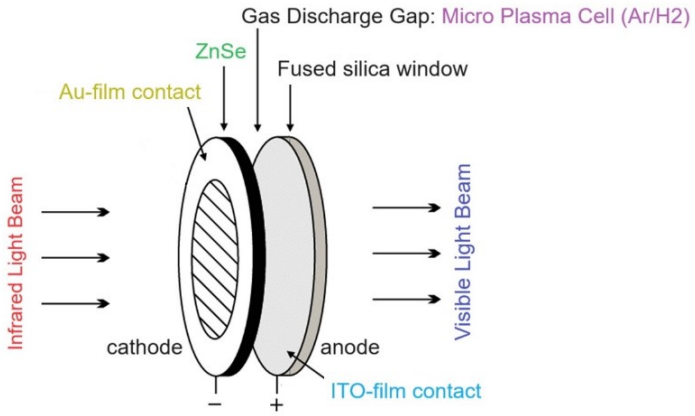

Figure 1. Sketch of GDSS cell, intended for infared-to-visible wavelength conversion application.

2. MATERIAL AND METHOD

The gas discharge-semiconductor microplasma (GDSμP) system was modeled and simulated in 2D media. The surface of the semiconductor cathode electrode, exposed to infrared (IR) light beam, was coated with thin gold (Au) film as electrical contact element. The surface of the fused-glass substrate of the anode electrode, exposed to glow light emissions (GLE), was coated with thin ITO film as electrical contact element.

Type II-VI compound semiconductor zinc selenide (ZnSe) as the cathode material was modeled in comb-plate style with micro-digitated electron emission surface, coupled to a micro discharge gap of unary argon (Ar) and binary argon/hydrogen (Ar/H_2) gases. The binary gas system consisted of Ar mixed with 10% molar H_2 gas. A two-dimensional square chamber with 100 μm long discharge gap was introduced in unary Ar and binary Ar/H_2 gases at 250 Torr sub atmospheric pressure. Microscale normal glow discharges were generated under electric field fed with a constant voltage of 1300 VDC in a virtual electrical equivalent circuit (EEC) in the simulation platform.

Numerical analyzes of gas discharge-semiconductor microplasma (GDSμP) systems were performed in the COMSOL Multiphysics program using the electron energy distribution function. Microplasma simulations were run to explore the fast transient discharge parameters, including electron density (ED), electron current density (ECD), and electric potential (EP). The variables in the GDSμP system simulation runs are tabulated in Table 1.

Table 1. The variables in the GDSμP system simulation runs.

Parameter	**Value/Description**
Voltage between electrodes (anode-to-cathode)	V = 1300 VDC
Gas types	Ar and Ar/H_2 (10%)
Gas pressure	P = 250 Torr
Distance between electrodes (anode-to-cathode)	d = 100 μm
Cathode electrode material type	ZnSe with micro-digitated surface
Cathode electrode diameter	D = 100 μm
Anode electrode material type	ITO-film coated SiO_2 window
Density of initial (seed) electrons in the gas discharge medium	$n_{e,o}$ = 1E17 ($1/m^3$)
Paschen product	P.d = 2.5 Torr.cm
Ambient operating temperature of GDSμP cell	T = 300 K

The physical and mesh structures of GDSμP cell model are shown in Figure 2.

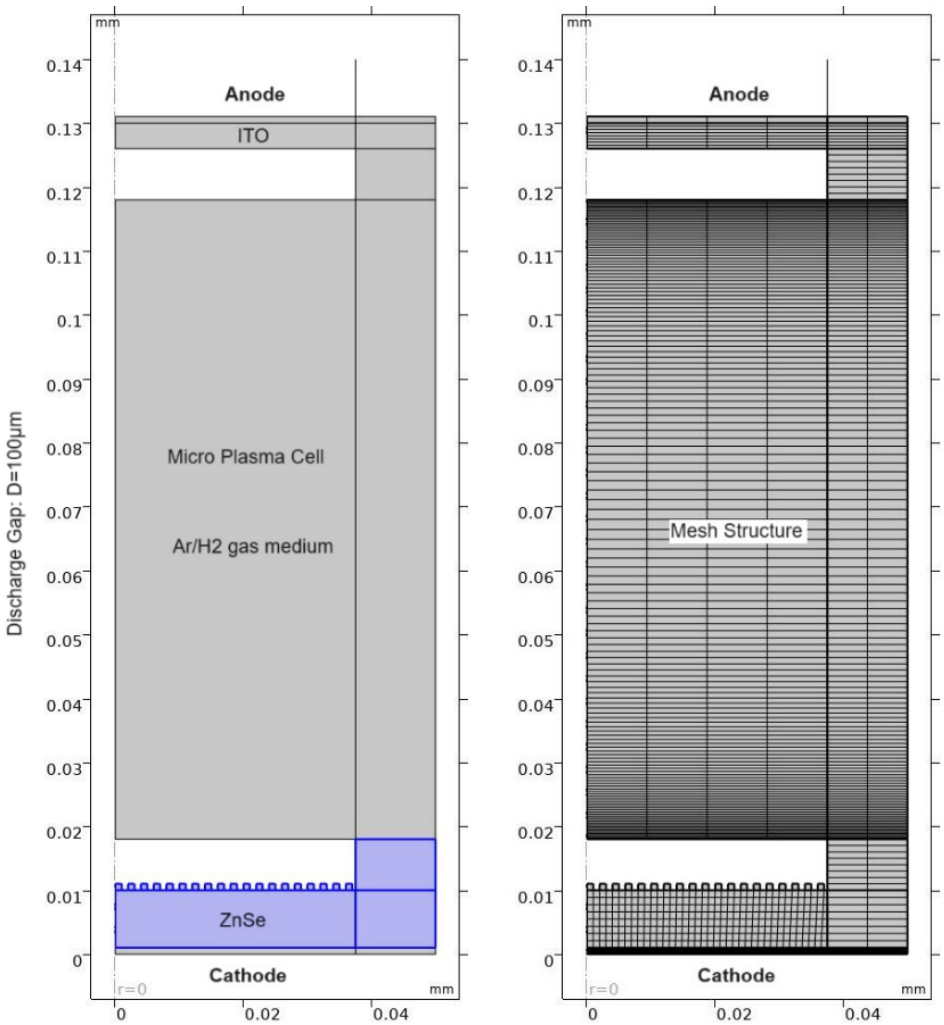

Figure 2. Sketch of GDSµP cell model in 2D layout: (a) Physical structure, and (b) Mesh structure.

3. RESULTS

In Figure 3, the spatiotemporal distributions of the electron density (ED) parameter data obtained across 100 µm long discharge gap were plotted as curves, respectively for; (a) initial phase of unary Ar -system, (b) initial phase of binary Ar/H_2 -system, (c) final phase of unary Ar -system, (d) final phase of binary Ar/H_2 -system, (e) full period of unary Ar -system, and (f) full period of binary Ar/H_2 -system.

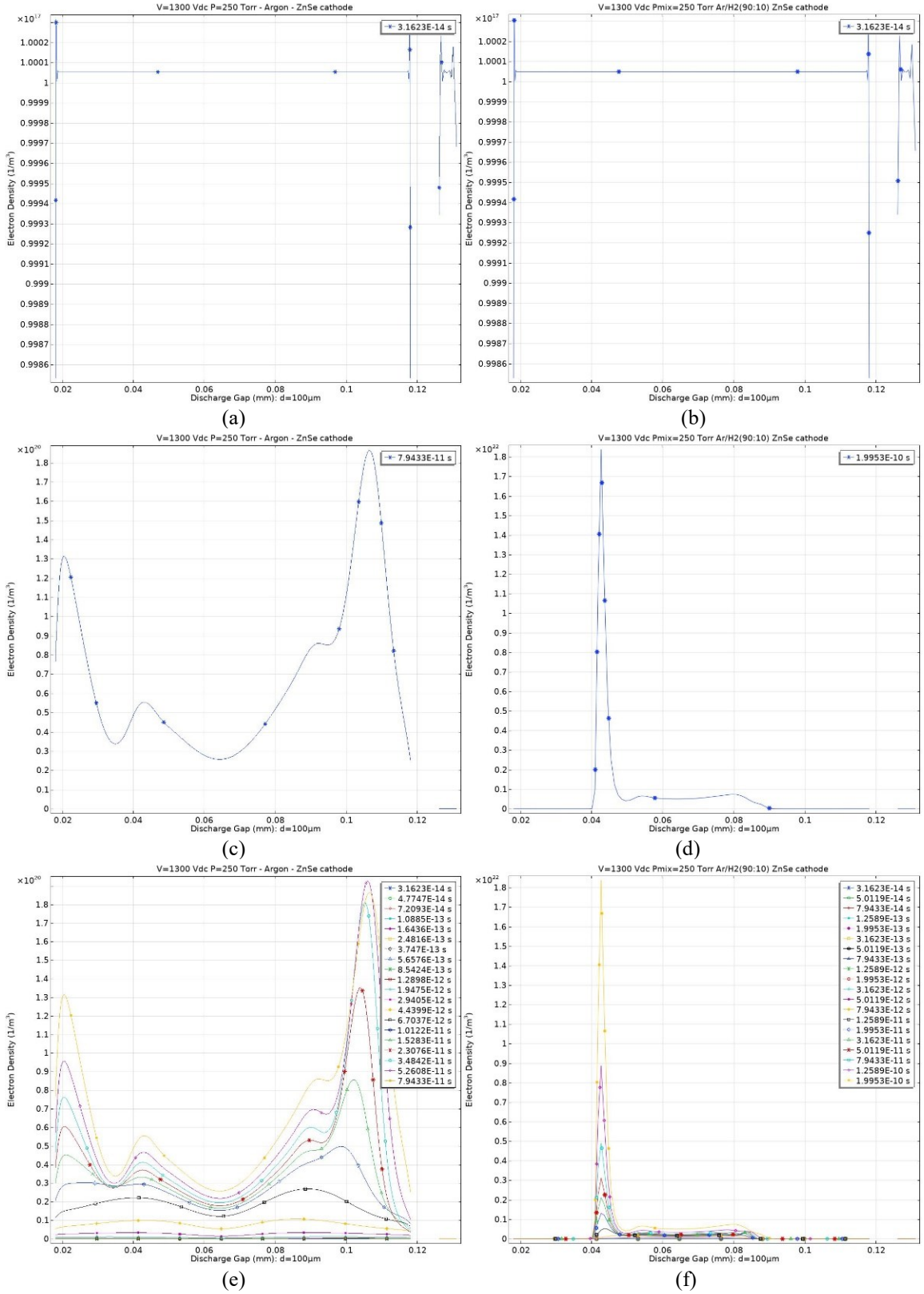

Figure 3. Spatiotemporal distributions of electron density (ED) data across 100 µm long discharge gap, respectively for; (a) initial phase of unary Ar -system, (b) initial phase of binary Ar/H_2(90:10) -system, (c) final phase of unary Ar -system, (d) final phase of binary Ar/H_2 (90:10) -system, (e) full period of unary Ar -system, (f) full period of binary Ar/H_2 (90:10) -system.

In Figure 4, the spatial distributions of the electron density (ED) parameter data obtained across 100 µm long discharge gap are shown in 3D images, respectively for; (a) final phase of unary Ar -system, and (b) final phase of binary Ar/H_2 (90:10) -system.

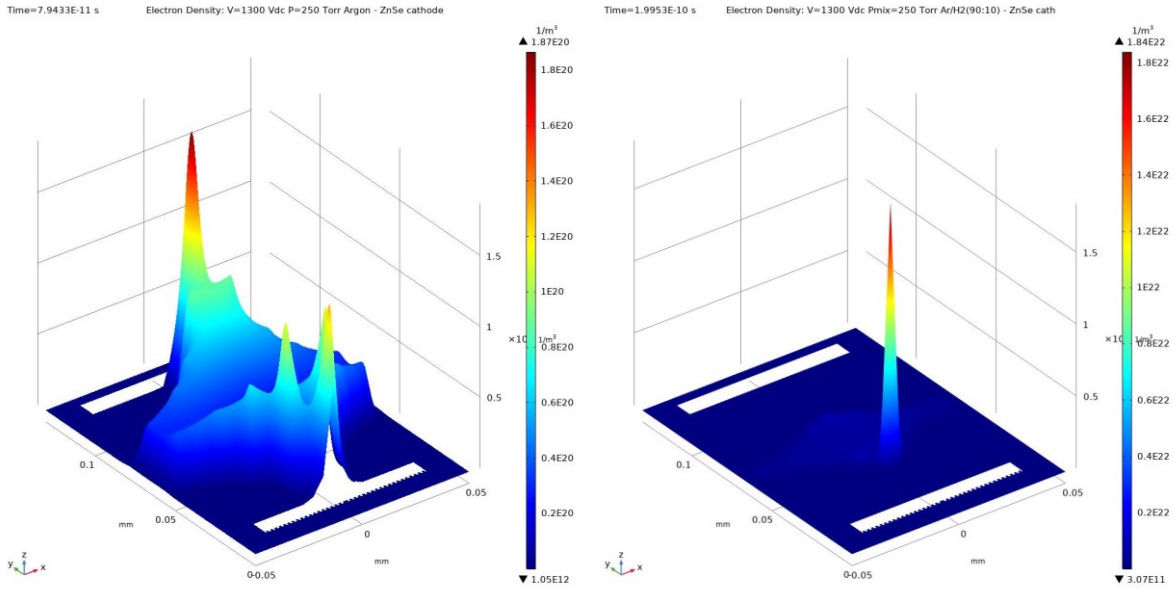

(a) (b)

Figure 4. Spatial distributions of electron density (ED) data obtained across 100 µm long discharge gap in 3D images, respectively for; (a) final phase of unary Ar -system, (b) final phase of binary Ar/H_2 (90:10) -system.

In Figure 5, the spatial distributions of the electron current density (ECD) parameter data obtained across 100 µm long discharge gap are shown in 3D images, respectively for; (a) final phase of unary Ar -system, and (b) final phase of binary Ar/H_2 (90:10) -system.

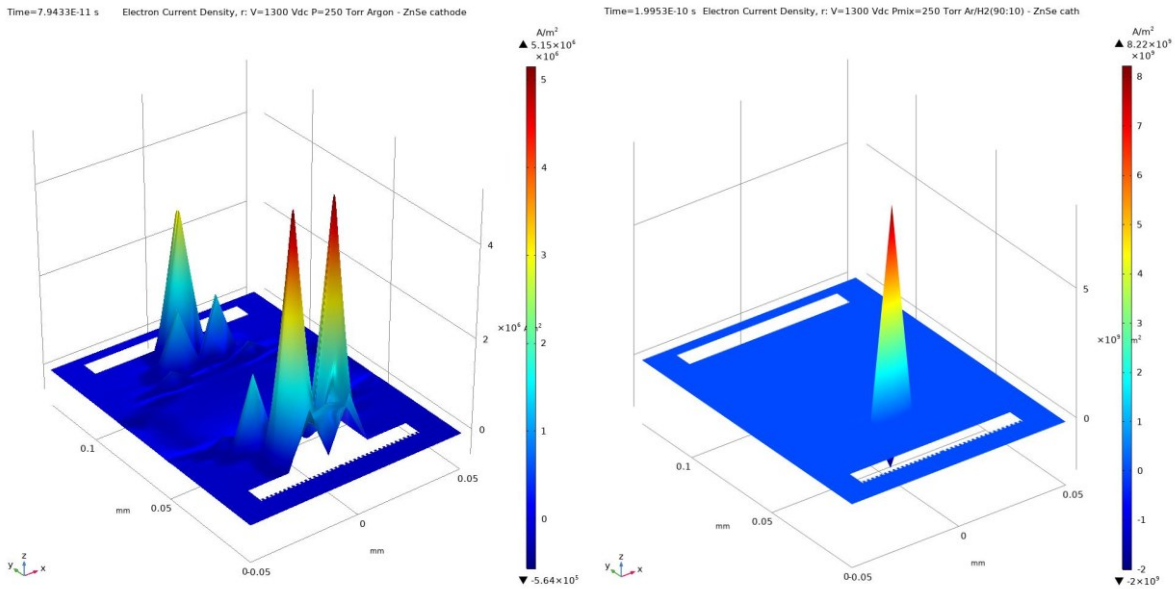

(a) (b)

Figure 5. Spatial distributions of electron current density (ECD) data obtained across 100 µm long discharge gap in 3D images, respectively for; (a) final phase of unary Ar -system, (b) final phase of binary Ar/H_2 (90:10) -system.

In Figure 6, the spatial distributions of the electric potential (EP) parameter data obtained across 100 µm long discharge gap are shown in 3D images, respectively for; (a) final phase of unary Ar -system, and (b) final phase of binary Ar/H_2 (90:10) -system.

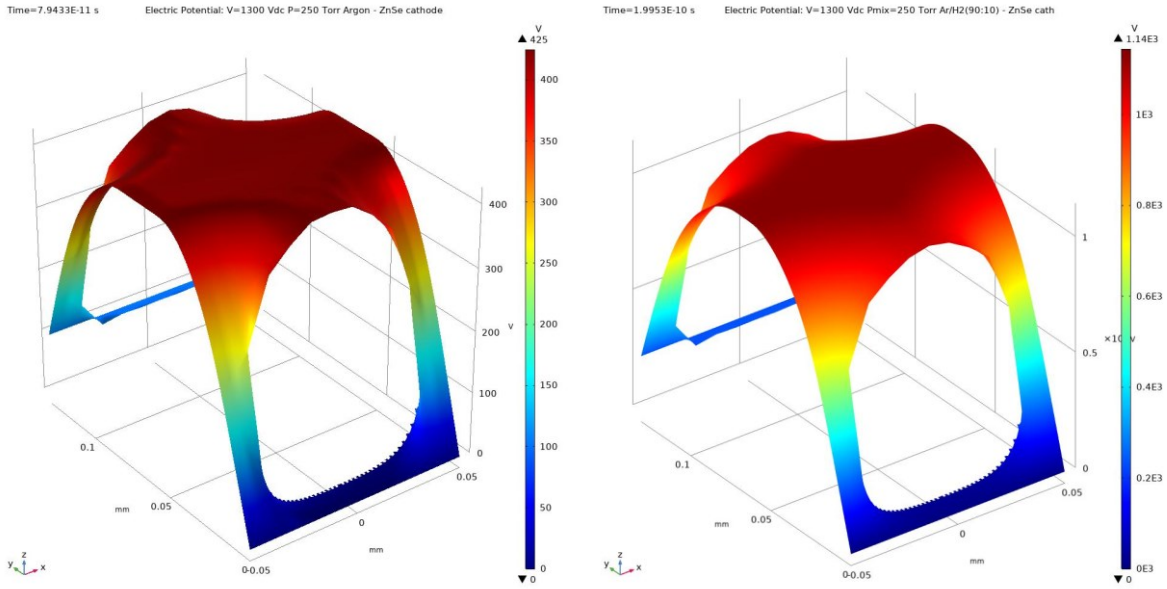

(a) (b)

Figure 6. Spatial distributions of electric potential (EP) data obtained across 100 µm long discharge gap in 3D images, respectively for; (a) final phase of unary Ar -system, (b) final phase of binary Ar/H_2 (90:10) -system.

Table 2 summarizes the comparative data of discharge parameters, including electron density, electron current density, and electric potential for unary Ar and binary Ar/H_2 (90:10) -systems.

Table 2. Comparative data of discharge parameters: Unary argon (Ar) and binary argon/hydrogen (Ar/H_2) -systems.

Parameter	**Unary Ar -system**	**Binary Ar/H_2 (90:10) -system**
SS_o	Simulation run started at time (s):	
	$3.1623x10^{-14}$	$3.1623x10^{-14}$
SS_f	Simulation run ended at time (s):	
	$7.9433x10^{-11}$	$1.9953x10^{-10}$
$ED_{i,0}$	Initial Electron Density ($1/m^3$):	
	$1.0x10^{17}$	$1.0x10^{17}$
$ED_{f,p}$	Electron Density at the final phase, peak ($1/m^3$):	
	$1.87x10^{20}$	$1.84x10^{22}$
$ECD_{f,p}$	Electron Current Density at the final phase, peak (A/m^2):	
	$5.15x10^{6}$	$8.22x10^{9}$
$EP_{f,p}$	Electric Potential at the final phase, peak (V):	
	425	1140

According to the numerical analyzes conducted within the scope of this study;

Referring to the data summarized in Table 2 for unary Ar and binary Ar/H_2 (90:10) -systems of the proposed GDSµP simulation model, the following comparative results were obtained:

- Simulation runs of unary Ar and binary Ar/H_2 -systems were started at the same time in seconds; SS_o.
- Binary Ar/H_2 -system stabilized slightly longer in time than unary Ar -system; SS_f.
- Initial electron density value was set the same for both unary Ar and binary Ar/H_2 -systems; $ED_{i,0}$.
- Peak electron density value at the final phase of the discharge period for binary Ar/H_2 -system was 100 times higher than that for unary Ar -system, $ED_{f,p}$.
- Peak electron current density value at the final phase of the discharge period for binary Ar/H_2 -system was 1000 times higher than that for unary Ar -system, $ECD_{f,p}$.

- Peak electric potential value at the final phase of the discharge period for binary Ar/H_2 -system was 1140 VDC, higher than that for unary Ar -system 425 VDC, $EP_{f,p}$.

In Figure 7, the Paschen curves are shown for argon and hydrogen gas discharges [3]. The static breakdown voltage (V_B) of a gas medium is defined by the product of gas pressure (***P***, Torr) and inter-electrode gap distance (***d***, cm), corresponding to ***P.d*** in Torr.cm. In this study, the ***P.d*** product corresponding to 2.5 Torr.cm is marked by the vertical dot line on the Paschen curves of argon and hydrogen gasses.

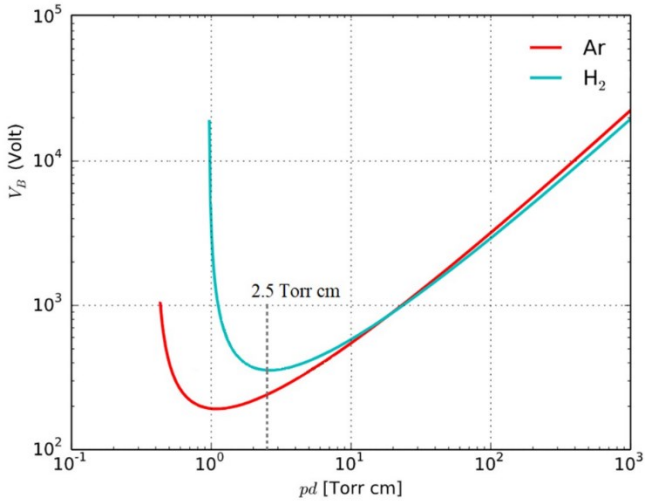

Figure 7. The ***P.d*** product corresponding to 2.5 Torr.cm, marked on the Paschen curves of Ar and H_2 gasses [3].

In Figure 8, the voltage-current (V-I) curve for a typical gas discharge system is shown [13]. The peak discharge currents of the simulation runs were estimated to be approximately 0.5 mA for unary Ar -system and 10 mA for binary Ar/H_2 -system, lying in the normal glow discharge regime of the V-I curve.

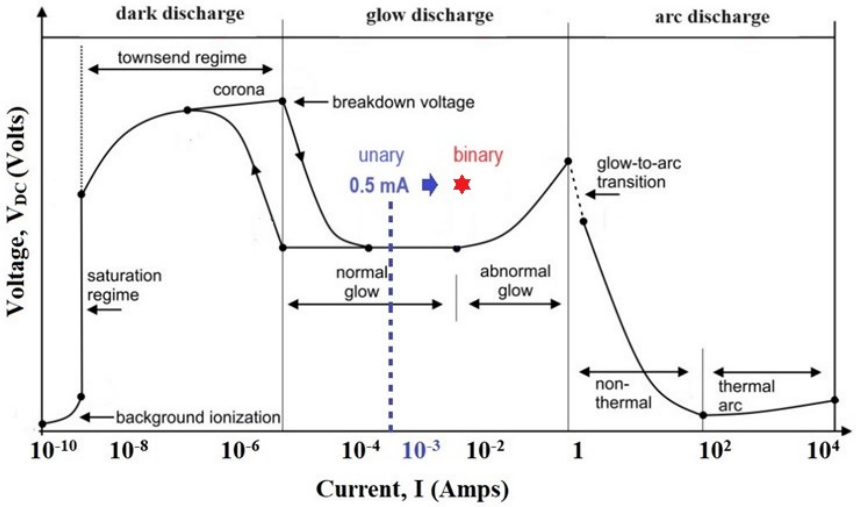

Figure 8. Peak discharge currents of unary Ar and binary Ar/H_2 -discharge systems, lying in the normal glow discharge regime of the V-I curve [13].

By adding hydrogen to argon, forming binary Ar/H_2 -system, the calculated peak discharge current was located in the upper part of the normal glow discharge region, which theoretically did not extend to the abnormal glow discharge region for the electrical stability of the semiconductor-gas discharge microplasma system.

4. CONCLUSION

The spatiotemporal distributions of the electron density and the electron current density parameters in binary Ar/H_2 -system were locally more concentrated and numerically stronger than in unary Ar -system as discharge reactions progressed over the discharge period. The peak electron density value at the final phase of the discharge period for binary Ar/H_2 -system was 100 times higher than that for unary Ar -system. The peak electron current density value at the final phase of the discharge period for binary Ar/H_2 -system was 1000 times higher than that for unary Ar -system.

It was revealed that by adding hydrogen to argon, the electrical stability of ZnSe cathode material and the spatiotemporal distribution uniformity of glow-discharge emissions were enhanced over the discharge period of the fast-transient microplasma

reactions. The safe operating voltage of a microplasma device for a given microgap can be precisely tuned on the Paschen curve by adding hydrogen at an appropriate molar fraction to argon at a well-defined pressure level. It was figured out that gas discharge-semiconductor microplasma (GDSμP) systems can be specifically designed for the infrared detector and image converter device applications.

ACKNOWLEDGEMENT

The Scientific Research Projects Coordination Unit of Gazi University supported this study with the project number FDK-2023-8704.

ETHICAL STANDARD DECLARATION

It was declared by the authors that the materials and methods used in this article do not require any ethics committee permission.

AUTHORS' CONTRIBUTIONS

Erhan ONGUN: Modeling, numerical analysis, article writing.
Prof. Dr. Hatice Hilal YÜCEL (KURT) : Supervisor of EO's doctoral thesis, expert on the plasma science and technology, numerical analyses, article writing and editing.

CONFLICT OF INTEREST

There is no conflict of interest in this study.

DATA AVAILABILITY STATEMENT

The supplementary data for this article can be requested from the corresponding author.

REFERENCES

[1] Schoenbach, K.H., Becker, K. (2016). 20 years of microplasma research: A status report. *Eur. Phys. J. D*, 70, 29.
[2] Chiang, W.-H., Mariotti, D., Sankaran, R.M., Eden, J.G., Ostrikov, K. (2020). Microplasmas for advanced materials and devices. *Adv. Mater.*, 32, 1905508.
[3] Azar, M.T., Pai, P. (2017). Microplasma field effect transistors. *Micromachines*, 8(4), 117.
[4] Kurt, H.H., Koc, E., Salamov, B. (2010). Atmospheric pressure DC glow discharge in semiconductor gas discharge electronic devices. *IEEE Transactions on Plasma Science*, 38(2), 137.
[5] Sadiq, Y., Kurt, H.Y., Albarzanji, A.O., Alekperov, S.D., Salamov, B.G. (2009). Transport properties in semiconductor-gas discharge electronic devices. *Solid-state electronics*, 53(9), 1009.
[6] Garner, A.L., Meng, G., Fu, Y., Loveless, A.M., Brayfield II, R.S., Darr, A.M. (2020). Transitions between electron emission and gas breakdown mechanisms across length and pressure scales. *J. Appl. Phys.*, 128, 210903.
[7] Go, D.B., Venkattraman, A. (2014). Microscale gas breakdown: ion-enhanced field emission and the modified Paschen's curve. *J. Phys. D: Appl. Phys.*, 47, 503001.
[8] Garner, A.L., Loveless, A.M., Dahal, J.N., Venkattraman, A. (2020). A tutorial on theoretical and computational techniques for gas breakdown in microscale gaps. *IEEE Transactions on Plasma Science*, 99:1-17.
[9] Donald, D.H., Hendrik, C.S., Setumo, V.M., Lehlohonolo, F.K. (2022). *Zinc selenide semiconductor: synthesis, properties and applications. Nanoscale Compound Semiconductors and their Optoelectronics Applications*, Woodhead Publishing Series in Electronic and Optical Materials, 67-84. https://doi.org/10.1016/B978-0-12-824062-5.00001-4.
[10] Morkoc, B.H., Strite, S., Gao, G.B., Lin, M.E., Sverdlov, B., Burns, M. (1994). Large-band-gap SiC, III-V nitride, and II-VI ZnSe-based semiconductor device Technologies. *Journal of Applied Physics*, 76(3), 1363.
[11] Kurt, H.H., Tanrıverdi E. (2017). Electrical Properties of ZnS and ZnSe Semiconductors in a plasma-semiconductor system. *Journal of Electronic Materials*, 46(7), 3965.
[12] Kurt, H.H. (2018). Exploration of gas discharges with GaAs, GaP and ZnSe electrodes under atmospheric pressure. *Journal of Electronic Materials*, 47, 4444.
[13] Ongun, E., Yücel (Kurt), H.H., Utaş, S. (2024). DC-driven subatmospheric glow discharges in the infrared-stimulated. *J Mater Sci: Mater Electron*, 35:655, https://doi.org/10.1007/s10854-024-12382-1.
[14] Brayfield II, R.S., Fairbanks, A.J., Loveless, A.M., Gao, S., Dhanabal, A., Li, W., Darr, C., Wu, W., Garner, A.L. (2019). The impact of cathode surface roughness and multiple breakdown events on microscale gas breakdown at atmospheric pressure. *J. Appl. Phys.*, 125, 203302.
[15] Fu, Y., Zhang, P., Krek, J., Verboncoeur, J.P. (2019). Gas breakdown and its scaling law in microgaps with multiple concentric cathode protrusions. *Appl. Phys. Lett.*, 114, 014102.
[16] Kurt, H.Y., İnaloz A., Salamov, B.G. (2010). Study of non-thermal plasma discharge in semiconductor gas discharge electronic devices. *Optoelectronics and Advanced Materials-Rapid Communications*, 4, 205.